International Journal of Modern Physics B
Vol. 38, No. 26 (2024) 2450353 (14 pages)

DOI: 10.1142/S0217979224503533

World Scientific
www.worldscientific.com

A new type of supercontinuum generation in hexagonal lattice C_6H_6-core PCF with broadband and low-power pump

Bao Tran Le Tran* and Lanh Chu Van†

Department of Physics, Vinh University,
182 Le Duan, Vinh City 461010, Vietnam
**letranbaotran212@gmail.com*
†*chuvanlanh@vinhuni.edu.vn*

Received 29 December 2022
Revised 9 May 2023
Accepted 25 June 2023
Published 21 September 2023

Most of the spectral bandwidths of previous publications are still limited by high input powers making them economically less than ideal. By using a benzene core (C_6H_6) photonic crystal fiber (PCF) as a new supercontinuum (SC) light source, it is possible to achieve a very large spectral broadening with hundreds of times lower peak power. Due to the change in the diameter of air holes in the first ring near the core, near-zero flattened dispersion, high nonlinearity and small attenuation can be achieved for spectral broadening. The structural geometries of two C_6H_6-PCFs are optimized to generate wide SC at low input energy. The SC spectrum produced in 1 cm long of all dispersion fiber extends from a part of visible light to the near-infrared range at 1.3 μm wavelength and a small pulse energy of 18 pJ (or 450 W of electrical input). The second PCF shows wide soliton-induced SC from 0.8 to 4.2 μm with 71 pJ pulse energy (or input power approximately 790 W) at 1.5 μm wavelength within a fiber of 12 cm. The proposed structures have the potential to become a new class of microstructured optical fibers for low-cost, broad-spectrum SC generation.

Keywords: Benzene-core photonic crystal fibers; flat near-zero dispersion; low attenuation; high nonlinearity; large supercontinuum spectral width; low peak power.

PACS numbers: 42.65.−k, 42.81.−i

1. Introduction

The light utilization in various fields of optics, i.e., all-optical network communication, sensors and medical diagnostics has led to the invention of a waveguide medium called optical fiber.[1] Accordingly, a new fiber type known as photonic crystal fiber (PCF) are realized. Day by day PCF has gradually replaced conventional optical fibers by alleviating their limitations.[2] In principle, PCFs work primarily in two following ways. First, light propagates through the entire solid core using modified

† Corresponding author.

total internal reflection.[3] Second, the hollow-core fiber guides the light directly into a core medium with a low refractive index on the basis of photonic bandgap effect.[4,5]

In recent years, several exciting studies have been carried out in solid-core fibers for various applications.[6,7] However, it is usually difficult to change the optical features of these PCFs to be tunable optical devices. Therefore, the efforts are focused on using liquids with a highly transparent and high nonlinear index to enhance the nonlinearity with adjustable dispersion,[8,9] see Fig. 1. It may be noted that a high nonlinear refractive index is required for SC generation.[10]

Currently, the development of PCFs with silica glass (SiO_2) and soft glasses is becoming a popular approach for SC generation applications. SiO_2-PCF is a good candidate to generate SC in the near-infrared (IR) region. Whereas, soft glass PCFs reportedly enabled pulse-preserving in the mid-IR. However, the low nonlinearity of SiO_2 limits SC broadening in these fibers.[11] On the other hand, optical fibers based on soft glass typically require complex pumping system to deliver sub-100 fs pulses.[12] Therefore, highly nonlinear liquid-filled PCFs have been explored as an alternative solution. Due to the high nonlinearity and high transparency of the selected liquids, the spectral width of SC light in liquid-core fibers from visible to the near-IR range can be achieved with low energies of pump pulses for short fiber samples.[9,13] Leaks can occur when liquid is filled with the PCF core. Nevertheless, these can be repaired by modern techniques such as two-photon direct laser writing techniques[14] or the UV-adhesive method.[15]

Several publications have reported SC generation in fibers with liquid cores. Using a very high pulse power of 55 kW, Lanh *et al.*[11] reported SC generation wider than two octaves in a C_6H_6-filled core fiber. Hieu *et al.*[18] measured SC generation in tetrachloroethylene-core (C_2Cl_4) PCF over a wavelength of 0.8–2 μm with normal dispersion. An improved method for selective liquid filling into fiber microstructures was considered,[19] which led to interesting near-IR soliton dynamics in hollow-core PCF structures infiltrated by 1,2-dibromoethane ($C_2H_4Br_2$). Spectral broadening was observed with large peak power (12.5 kW). The filling of carbon disulfide (CS_2) into the fiber core with two zero-dispersion wavelengths (ZDW) allowed the

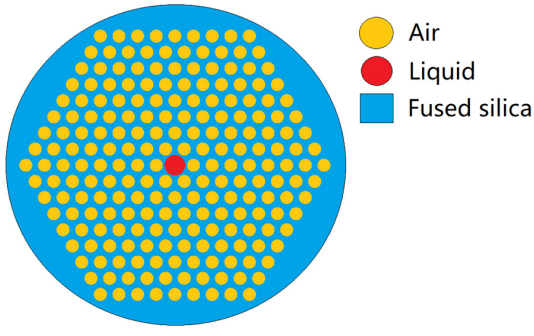

Fig. 1. (Color online) The hollow-core PCF structure infiltrated with liquid.

Table 1. Simulation results of SC generation in hollow-core PCFs infiltrated with liquid.

	Pulse parameters			PCF parameters			SC generation parameters		
#	Wavelength	Pulse power	Pulse duration	PCF structures	ZDW	Fiber length	SC range	Regime	Refs.
1	1.56 μm	55 kW and 18.5 kW	90 fs	C_6H_6-PCFs	1.557 μm	1 cm	0.7–2 μm and 0.6–2.6 μm	All-normal and anomalous	11
2	1.55 μm	0.56 kW	100 fs	C_7H_8-PCF	1.523 μm	10 cm	0.911–2.496 μm	Anomalous	16
3	0.532 μm	11.11 kW	18 ps	C_7H_8-PCF	—	5 cm	0.55–0.87 μm	All-normal	17
4	1.56 μm	16.67 kW	40 fs	C_2Cl_4-PCFs	1.5 μm	5 cm and 10 cm	0.8–2 μm and 1–2 μm	All-normal and anomalous	18
5	1.03 μm	12.5 kW	40 fs	$C_2H_4Br_2$-PCF	—	10 cm	0.64–1.7 μm	All-normal	19
6	1.95 μm	3.043 kW	460 fs	CS_2-PCF	1.3 μm	15 cm	1.1–2.7 μm	Anomalous	20
7	1.92 μm	1.428 kW	350 fs	CS_2-PCF	1.3 μm and 2.1 μm	5 cm	1.2–3 μm	Anomalous	21

generation of SC from the 1.2 to 3 μm range.[21] A summary of previous results on SC generation of different liquid-filled fibers is shown in Table 1.

Most of the works above use PCF with the same air hole diameter for the rings. Unfortunately, uniform PCFs usually optimize only the dispersion properties and not the loss or nonlinear coefficients, although they are very practical during fiber fabrication. Moreover, the spectral bandwidths in these cases are still limited by high input powers and long fiber lengths, making them economically less than ideal.

To overcome the above limitations, in this study, we design a C_6H_6-infiltrated hollow-core PCF for SC generation. With the goal of generating a broadband coherent SC spectrum from the visible to the mid-IR at very low input power, the PCF cross section was specifically designed to accommodate different diameters of the air holes in the rings. This results in a flat dispersion profile and near-zero dispersion wavelength, high nonlinearity and minimal attenuation. A hexagonal lattice is chosen for the study because of its advantages from the dispersion curves demonstrated in previous publications.[17,19,20] We emphasize using C_6H_6 as the filling material for the fiber core because C_6H_6 has a high nonlinear refractive index, $n_2 = 168 \times 10^{-20}\,\mathrm{m^2/W}$ at 1.064 μm. When compared with liquids commonly used in practice, this value is significantly higher than that of carbon tetrachloride and chloroform. It also corresponds to the nonlinear refractive index of C_7H_8 and nitrobenzene.[11,16,22] This advantage and the transparent window in the broadband range from 0.5 to 1.4 μm make C_6H_6 a promising material for SC generation in liquid-filled PCFs.[11]

2. Numerical Modeling and Simulation Results

The goal of this section is to design a suitable liquid glass structure that allows the optimization of optical property parameters. We examine a typical PCF performed

by Saitoh *et al.*[23] The hexagonal lattice model is flexibly changed to study the influence of the air-hole diameter parameter in each ring on characteristic quantities of the fiber (Fig. 2(a)). We flexibly modify the hexagonal lattice model to investigate the effect of the air-hole diameter parameter of each ring on the characteristics of the fiber. The results obtained after a series of simulations show that the dispersion characteristics are dominated by the first air-hole ring. Meanwhile, the mode properties are controlled by the other rings.[23] Therefore, we design the holes in the first ring with diameter d_1 and filling factor ($f_1 = d_1/\Lambda$) varying in the 0.3–0.8 range in steps of 0.05 (Fig. 2(b)). The air-filling factor ($f_2 = d_2/\Lambda$) for the other rings is assumed to be 0.95. The core diameter is given by the following formula: $D_c = 2\Lambda - 1.1d_1$, where lattice constant Λ is taken from 1.0 to 2.5 μm in steps of 0.5. It is very difficult to simultaneously control the PCF properties in previous models.[6,18,24] Thus, creating fibers with optimal chromatic dispersion and very low loss is an innovation and a major achievement of current designs. From the obtained structures, PCFs with flat dispersion of the fundamental mode are selected to calculate the linear and nonlinear optical parameters in the wavelength range of 0.5–2 μm.

It has already been emphasized in Sec. 1 that the use of C_6H_6 to penetrate the hollow core of PCF seems interesting. It is widely used in industry and daily life, such as making plastic, resins, synthetic fibers, rubber lubricants, gasoline and crude oil.[25] The material attenuation of C_6H_6 in the visible-to-near-IR region was experimentally measured using a halogen lamp and two spectrometers Ocean Near-IR-QUEST and Thorlabs CCS200 (see Fig. 3(a)). Figure 3(b) shows attenuation from 1.28 to 16 μm.[26]

Current designs assume SiO_2 glass as the substrate due to its high transparency and purity and ease of use in fiber manufacturing. The linear refractive indices of SiO_2 and C_6H_6 are described using the Sellmeier relation[27] and the Cauchy relation.[28] Their corresponding parameters are listed in Table 2. Mainly due to the fact that the

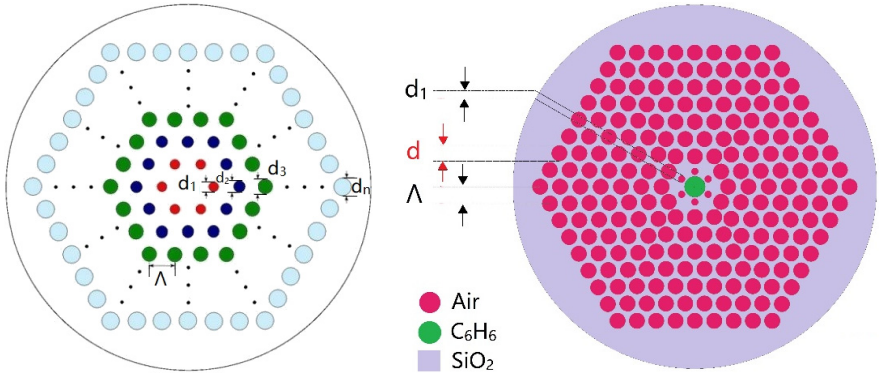

(a) (b)

Fig. 2. (Color online) Geometrical structure of PCFs: (a) Ref. 23 and (b) this work.

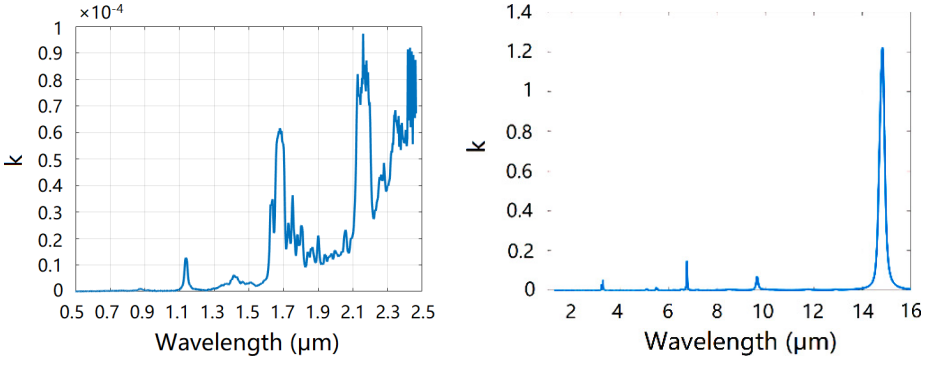

(a) (b)

Fig. 3. Attenuation of C_6H_6: (a) measured and (b) Ref. 26.

Table 2. Coefficients of the materials used.

$n^2(\lambda) = 1 + \frac{A_1\lambda^2}{\lambda^2-B_1} + \frac{A_2\lambda^2}{\lambda^2-B_2} + \frac{A_3\lambda^2}{\lambda^2-B_3}$, (1)		$n_b^2(\lambda) = C_0 + C_1\lambda^2 + \frac{C_2}{\lambda^2} + \frac{C_3}{\lambda^4} + \frac{C_4}{\lambda^6}$. (2)	
SiO_2		C_6H_6	
A_1	0.6694226	C_0	2.170184597
A_2	0.4345839	C_1	0.000593990 μm^2
A_3	0.8716947	C_2	0.023034640 μm^2
B_1	4.4801×10^{-3} μm^2	C_3	0.000499485 μm^4
B_2	1.3285×10^{-2} μm^2	C_4	0.000178796 μm^6
B_3	95.341482 μm^2		

refractive index of C_6H_6 is always larger than that of SiO_2 over the entire studied wavelength range, optical transmission in C_6H_6-filled PCFs follows a modified total internal reflection phenomenon as solid-core fibers, see Fig. 4.

The chromatic dispersion at different Λ and f_1 is numerically analyzed based on the finite-difference eigenmode (FDM). The cross section of PCF is divided into small rectangular sections, called "Yee mesh", which change the PCF properties very little. The possibility to control the lattice constant and filling factor allows accurate shaping of the chromatic dispersion properties in the whole wavelength range. As shown in Fig. 5, most fibers have anomalous dispersion from near-IR towards longer wavelengths except for the fiber with $\Lambda = 1.0\,\mu m$ and $f_1 = 0.5\,\mu m$. The dispersion curve of this fiber is completely located in the normal dispersion region and is very close to the zero-dispersion curve. A similar situation is also observed for fiber with $\Lambda = 1.0\,\mu m$ and $f_1 = 0.45\,\mu m$ regardless of the regime change. However, with the expectation of SC generation at $1.5\,\mu m$ close to the third fiber optic communication window ($\lambda_p = 1.55\,\mu m$) where the transmission loss is lowest, the PCF with $\Lambda = 2.5\,\mu m$ and $f_1 = 0.3\,\mu m$ is more satisfying because its ZDW is closest to the wavelength of the pump source, $1.47\,\mu m$. It is worth noting that we do not use

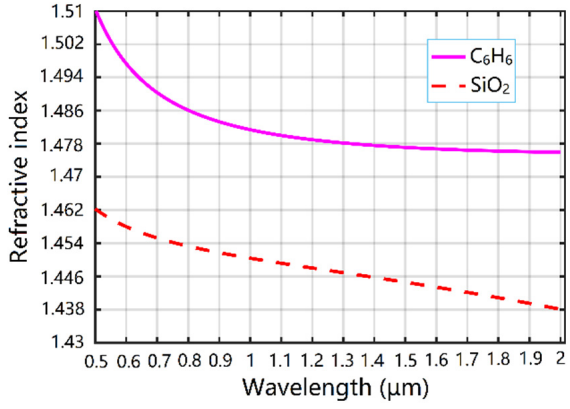

Fig. 4. (Color online) Refractive index of C_6H_6 and SiO_2.

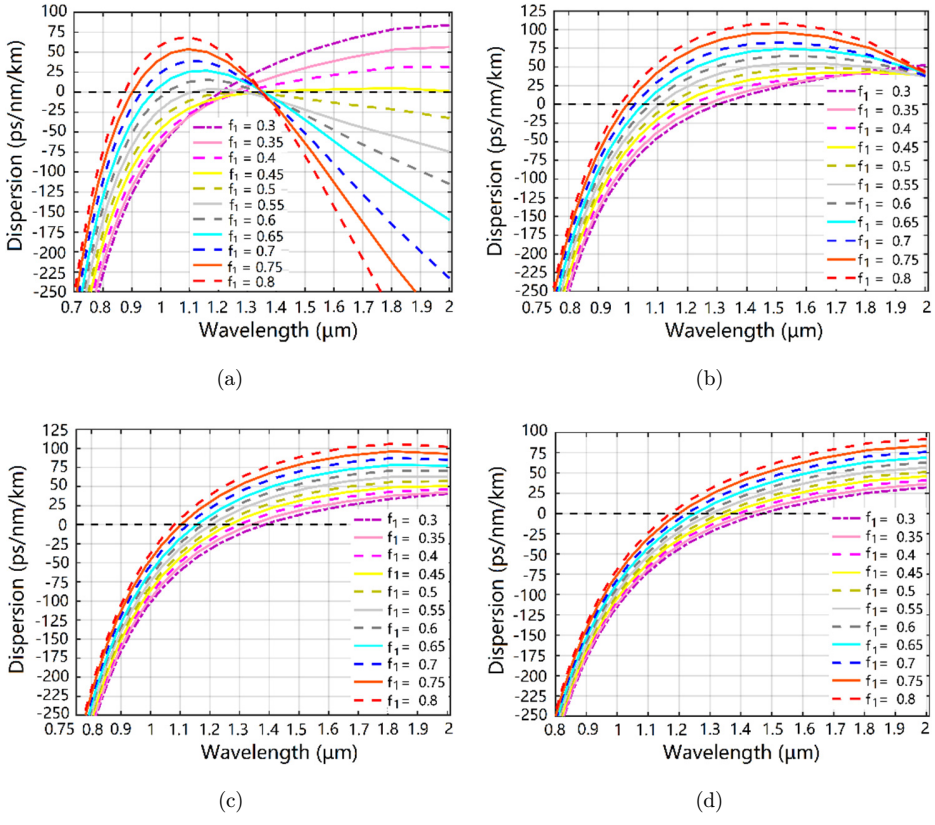

Fig. 5. (Color online) Dispersion characteristics of the C_6H_6-filled PCFs: (a) $\Lambda = 1.0\,\mu$m, (b) $\Lambda = 1.5\,\mu$m, (c) $\Lambda = 2.0\,\mu$m and (d) $\Lambda = 2.5\,\mu$m.

genetic algorithms and seed swarms to find the optimal structure to shorten the simulation time. The selection of optimal structures based on flat near-zero dispersion characteristics as above aims to improve the efficiency of SC and has been successfully applied in several publications.[16,19,22] It is well known that flat and near-zero dispersion is highly demanded for efficient SC generation. This makes it easy to enforce phase matching between different wave packets for an extended period of time producing new frequency components due to frequency mixing via cross-phase modulation (XPM) or four-wave mixing (FWM). Optimization algorithms are not used for the proposed structures because the structural parameters of PCFs are changed by a very small amount. This is perfectly suitable for PCF production because the error in fiber fabrication by the stack-and-drawn method is about 50 nm.[29] Therefore, two fibers with parameters $\Lambda = 1.0\,\mu$m, $f_1 = 0.5$ and $\Lambda = 2.5\,\mu$m, $f_1 = 0.3$ are selected for further analysis because of their potential for broadband SC generation.

From an experimental perspective, the stack-and-draw method and the procedure for selective liquid infiltration are used to fabricate the optimized structures. The manufacturing process has the following stages:

First, fused silica capillaries are gained by mechanical drilling on millimeter-sized solid rods. Second, they are stacked in a circular glass tube to stack a preform. The formed preform is successfully drawn into the fiber through precise control of the drawing speed, drawing temperature and lower rod speed to ensure the parameters of the designed fiber structures. In order to fill the core with a liquid, we use a thermal splicer with tailored electric arc energies and fusion times to fuse the outer rings of air holes. The core of the proposed fibers is then embedded into a liquid reservoir that is integrated with a microfluidic pump system. In such a system, C_6H_6 is infiltrated into the core of PCFs by capillary force and pressure from a microfluidic pump so that the liquid is kept in the core over a long time and to compensate for the evaporated liquids at the fiber ends.[22,30] It is also noted that the microfluidic system (e.g. shown in Ref. 31) makes low pressure (around 100 kPa) and the value of pressure is highly stable.[22,30,31] The coupling between the proposed fiber with a single-mode fiber can be carried out by using an alignment sleeve or a conventional fusion splicer.[32,33] The geometric parameters of the proposed PCF are shown in Table 3.

Figure 6 presents the dispersion characteristics of selected structures. It is known that the fiber dispersion depends on the material dispersion of C_6H_6 and SiO_2, as well as waveguide dispersion as shown in previous works.[21,22] However, waveguide

Table 3. Main geometrical parameters of the suggested PCFs for SC generation.

Parameters	Fiber 1	Fiber 2
Lattice constant Λ [μm]	1.0	2.5
Filling factor f_1	0.5	0.3
Core diameter D_c [μm]	1.45	4.175

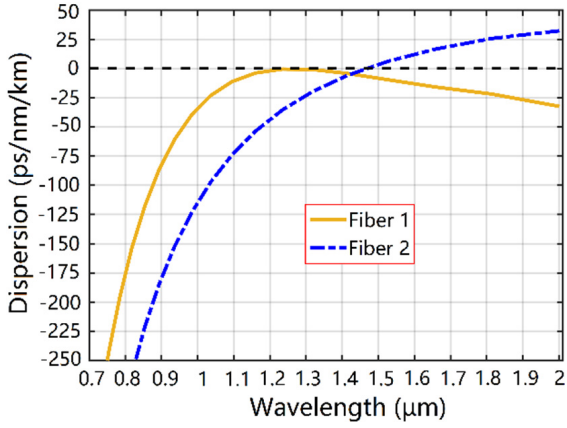

Fig. 6. (Color online) Dispersion curves of two proposed fibers.

dispersion has a significant influence on the fiber dispersion if the fiber has a small core in comparison with the wavelength (e.g., $D_c/\lambda < 2$). Meanwhile, the fiber with a large core has a dispersion shape following material dispersion of the core material (i.e., C_6H_6). For a case of small core fiber, the slight change in core diameter can visibly shift the fiber dispersion. Because of the significant influence of waveguide dispersion, the small core fiber (Fiber 1: $\Lambda = 1.0\,\mu$m, $f_1 = 0.5$) possesses a normal chromatic dispersion with an ultra-flat plateau of roughly between 1.1 and 1.4 μm. The fact that most small-core designs have a high confinement loss over the long-wavelength range limits spectral broadening. Nevertheless, SC generation with all-normal dispersion PCF has outstanding advantages that are widely aimed for since it makes the output pulses coherent and flat when the pumped wavelength is close to the wavelength of the maximum dispersion. This is one of our outstanding advantages compared to previous works.[18,21] Therefore, Fiber 1 is selected as one of the optimal fibers and is expected to pump at 1.3 μm. In contrast, Fiber 2 with $\Lambda = 2.5\,\mu$m, $f_1 = 0.3$ characterized mainly by material dispersion exhibits low anomalous dispersion for a wide range of wavelengths. Its ZDW is at about 1.489 μm. The central wavelength of the laser pump source of this fiber is 1.5 μm. In the proposed model, we took into account the effects of cladding SiO_2 on fiber loss. The fiber loss includes the material of C_6H_6 in the core, SiO_2 in the cladding and confinement loss. It is noted that C_6H_6 has a much higher linear refractive index than SiO_2, resulting in low confinement loss. Therefore, the fiber loss is approximately to sum of the material loss of C_6H_6 and light absorbed in the cladding by SiO_2, see Fig. 7. The attenuation curve (L_k) peaks at 1.66 μm for both structures, then they decrease sharply with increasing wavelength. On the other hand, this value is negligible in the short wavelength range. At the respective pumping wavelength, L_k is about 41.71 dB/m for Fiber 1 and 126.67 dB/m for Fiber 2. It is well known that for SCG, the high loss limits the spectral broadening and reduces the output intensity. However, this magnitude is still lower than that of some previous works.[16,34]

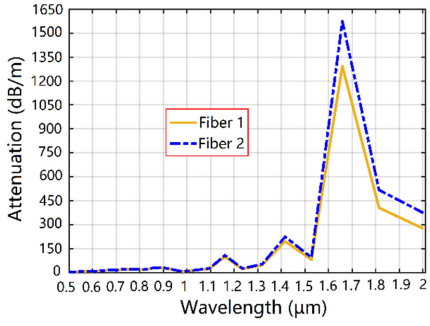

Fig. 7. (Color online) Attenuation curves of the proposed fibers.

Moreover, the effect of these fiber losses is not visible in the spectral broadening because the high nonlinear refractive index of C_6H_6 enables broad bandwidth of the SC spectrum induced in a short propagation (a few centimeters).

3. SC Generation in Optimized PCFs

For single-mode propagation, we use the generalized nonlinear Schrödinger[35]

$$\partial_z \tilde{A} - i\tilde{\beta}(\omega)\tilde{A} - \frac{\tilde{\alpha}(\omega)}{2}\tilde{A} = i\gamma\left(1 + \frac{\omega - \omega_0}{\omega_0}\right)\tilde{A}F\left[\int_{-\infty}^{+\infty} R(T')|A|^2(T - T')dT'\right]. \quad (3)$$

Equation (3) represents the transformation of the complex spectral envelope of the output pulse $\tilde{A}(\omega, z)$, where z is the spatial coordinate along the fiber. Loss ($\tilde{\alpha}$) and dispersion ($\tilde{\beta}$) linear operators correspond to the values measured in Figs. 6 and 7. The nonlinear effects are characterized by the Kerr nonlinearity coefficient $\gamma(\varpi) = 2\pi n_2/\lambda A_{\text{eff}}(\omega)$, pulse self-steepening $\tau = 1/\omega_0$, and Raman response function $R(T) = (1 - f_R)\delta(T) + f_R h_R(t)$.[10,36] Nonlinear parameter γ depends on the nonlinear refractive index of the C_6H_6 liquid and the effective mode area A_{eff}, see Fig. 8. As the wavelength increases, the light is no longer confined strongly inside the core because the modes get leaked through the holes, in between them increasing the effective mode area. Due to its large core diameter, the effective mode area of Fiber 2 is higher, and its nonlinear coefficient is lower than that of Fiber 1. In general, the two proposed PCFs have relatively large γ of 5256 and 960.02 $\text{W}^{-1}\,\text{km}^{-1}$ at 1.3 and 1.5 μm, respectively, thanks to the high nonlinear refractive index of C_6H_6. These values along with lower loss, flatter and smaller dispersion than previous publications[16,34,37] demonstrate the feasibility of C_6H_6 infiltration and the control of the parameters of the lattice geometry in shaping the optical characteristics as desired for SC generation.

For the proposed fibers, pulses with 1.3 μm wavelength, 40 fs duration (Fiber 1) and 1.5 μm, 90 fs (Fiber 2) are used based on Menlo Systems C-fiber femtosecond erbium laser. Regarding the thermal properties of the proposed optical fibers, further enhancing the pump power is a consideration during SC generation. The higher

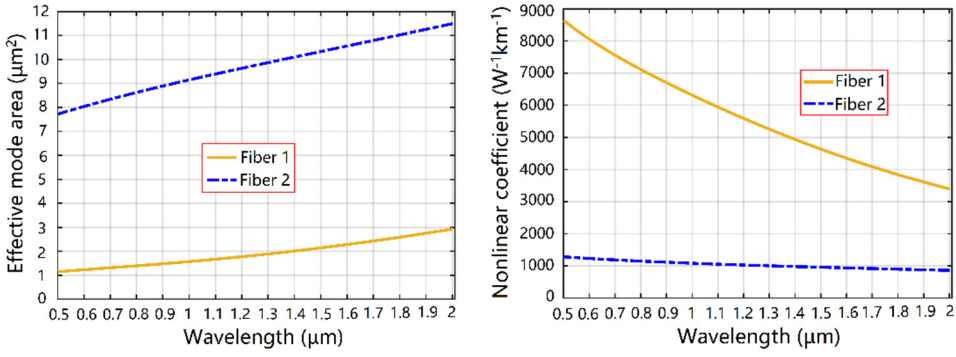

(a) (b)

Fig. 8. (Color online) (a) Effective mode area and (b) nonlinear coefficient for the optimized PCFs.

energy for the longer time can lead to the burning of C_6H_6.[21] We have carried out our numerical calculations for the proposed fibers with short lengths of 1 and 12 cm, the broad spectra generated with low peak power strongly depend on the all-normal and anomalous dispersion regime.

The all-normal dispersion SC generation in Fiber 1 is examined with different energy pulses. For a given input energy and dispersion shape, a bandwidth of self-phase modulation (SPM)-induced spectral broadening is determined by the spectral position of a pump wavelength. At an input pulse energy of 18 pJ (450 W peak power), the spectral bandwidth covers 0.72–1.82 μm within 5 dB dynamic ranges (Fig. 9(a)). The spectral broadening is caused by SPM in a few of the first centimeters of propagation from the onset. The high slope of normal dispersion limits the spectral broadening at the trailing edge. The spectrum becomes asymmetrical during further propagation. As observed in Fig. 9(b), OWB occurs first in the trailing edge of the pulse at 0. cm of propagation, creating a new band of the wavelength at

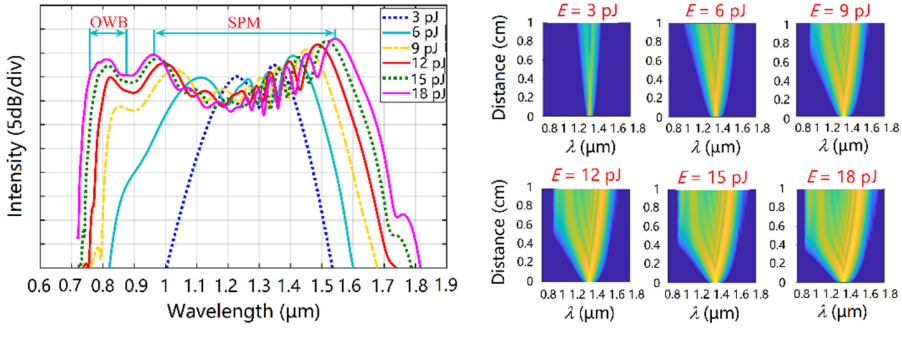

(a) (b)

Fig. 9. (Color online) (a) The output spectrum and (b) evolution of the SC along the fiber for various input pulse energy in 1 cm length when pumped with pulses of 40 fs duration, 1.3 μm pump wavelength, for Fiber 1.

0.72 μm. In the leading edge, the low value of dispersion (i.e. flat and close to zero) leads to the unclear observation of OWB. The generation of new wavelengths occurs through FWM where the short wavelength components propagate more slowly than the pulse tail part at the center.[38] The great effective mode area and small nonlinear coefficients at long wavelengths also limit further broadening. The appearance of OWB activates the energy transfer between different wavelength components which enhances the flatness of the central part of the spectrum. No soliton is formed herein because of not enough high energy. In addition, since modulation instability (MI) is suppressed in a normal dispersion regime, the all-normal dispersion SC, therefore, has high coherence over the whole observed spectrum. Pulses are maintained in the time domain with a smooth temporal profile, see Fig. 9(a). It is conceivable that the high coherence is that the SC generation is induced by SPM at the beginning of propagation in a normal dispersion regime and a small part of the spectrum is to form solitons in an anomalous dispersion regime when SMP-induced spectrum excess ZDWs. Here, MI does not play a significant role in amplifying the vacuum noise, thus the SC generation exhibits high coherence. Spectral broadening is completed at 1 cm.

In the case of Fiber 2, a ZDW exists at a wavelength of 1.47 μm. The 1.5 μm pump wavelength is within the anomalous dispersion range and close to the ZDW. Here, soliton self-frequency shift (SSFS) and soliton fission (SF)[39] play important roles in the broadband of the SC spectrum because of ultrashort pulse duration and low input energy. This point implies that the spectral position of the soliton can trigger the spectral bandwidth of the SC generation in the liquid core fibers. Dispersive waves (DW) help to create a new wavelength band when traversing the ZDW related to soliton shifting and OWB at the trailing edge. Whereas, SSFS causes the SC spectrum to shift to longer wavelengths, broadening the spectrum significantly towards redshifted wavelengths.[18]

Figure 10(a) shows the pulse spectra at various energies over Fiber 2 length of 12 cm. By increasing the input pump pulse energy, the SC spectrum broadens dynamically. Broadband SC spans from 0.78 to 4.13 μm at a 10 dB spectral level, wider than Fiber 1. The fact that increased SC bandwidth leads to an increase in noise sensitivity; it is for this reason that the spectral structures appeared to be complex as shown in Fig. 10(b). A large effective mode area (i.e., low nonlinear coefficient) restricts the soliton shifting as well as DW at the trailing edge. Consequently, no new wavelength is created during further propagation. Decreasing the pulse width and choosing the pump wavelength in the near-zero anomalous dispersion range can reduce noise amplification.[19] Before being influenced by SF, a part of the SPM-induced SC passes through the ZDW and is experienced in the normal dispersion region because of the proximity of the pump wavelength to ZDW (1.5 μm). Thus, it is stretched out with further flatness for the wing. It is possible to gain some insight into the spectral broadening dynamics through a quantitative comparison of parameters involved in various mechanisms during pulse propagation, namely the dispersive length L_D, nonlinear length L_{NL} and soliton number N.[10] For the peak power $P_0 = 789$ W corresponding to an energy of 71 pJ, pulse duration $t_0 = 90$ fs, and group

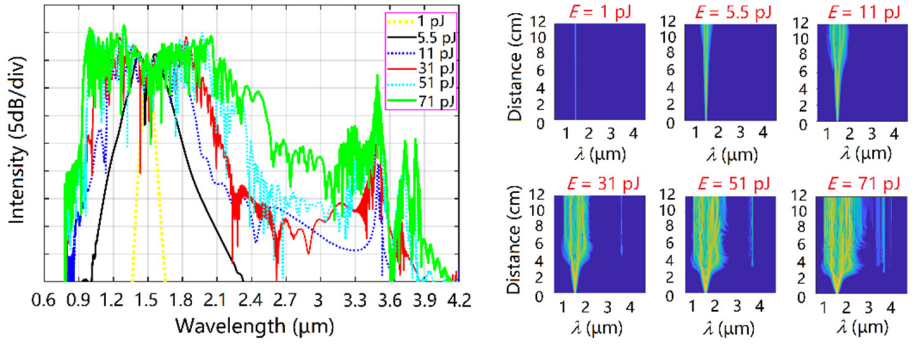

(a) (b)

Fig. 10. (Color online) (a) The output spectrum and (b) evolution of the SC along the fiber for various input pulse energies in 12 cm length when pumped with pulses of 90 fs duration, 1.5 μm pump wavelength, for Fiber 2.

velocity dispersion at the central wavelength $\beta_2 = -0.015\,\mathrm{ps}^2/\mathrm{m}$, the values for these scales are the following: $L_D = t_0^2/|\beta_2| = 54\,\mathrm{cm}$, $L_{\mathrm{NL}} = 1/\gamma P_0 = 0.13\,\mathrm{cm}$ and $N = \sqrt{L_D/L_{\mathrm{NL}}} = 20$. Therefore, SF ($L_{\mathrm{fiss}}$) and MI ($L_{\mathrm{MI}}$) property scales are defined as $L_{\mathrm{fiss}} = L_D/N = 2.7\,\mathrm{cm}$ and $L_{\mathrm{MI}} = 16L_{\mathrm{NL}} = 2.08\,\mathrm{cm}$. This means that SF started to appear after only 27 mm of propagation length with the assistance of FWM. Furthermore, the value of $L_{\mathrm{MI}} < L_{\mathrm{fiss}}$, i.e., the noise is amplified by MI occurs before the SF, proves the agreement of the spectral configuration obtained in Fig. 10.

The corresponding SC development over time is shown in Fig. 11. In any case, different frequency components usually have different group velocities. Therefore, the time delay between frequencies increases with longer propagation. On the other hand, the higher the pump pulse energy, the faster the time delay between different frequencies occurs over short distances. Although the SC is mainly induced by SPM

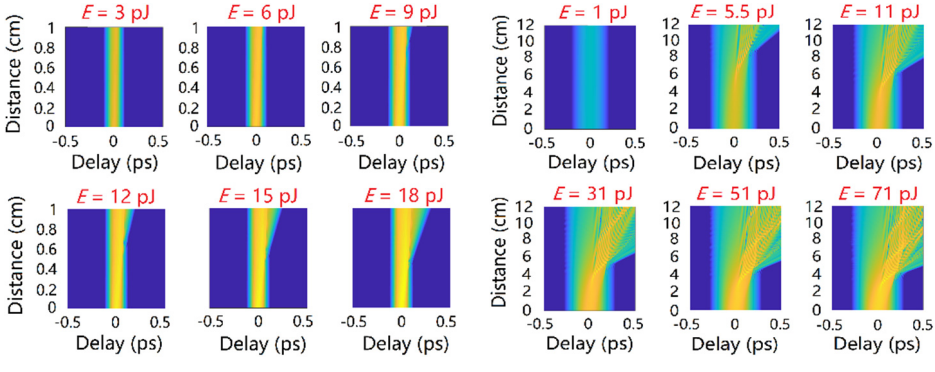

(a) (b)

Fig. 11. The temporal profile at different positions of the propagation length, respectively, with the spectrum growing along the suggestive fibers: (a) Fiber 1 and (b) Fiber 2.

and OWB for fiber with all-normal dispersion, the anomalous dispersion in the output light leads to further delay of the leading edge in the time domain, see Fig. 11(a). DW-induced and soliton-induced parts in the anomalous dispersion fiber have different delays, and they visibly separate each other as shown in Fig. 11(b). At a very short propagation distance, only a few millimeters of fiber length, SC generation occurs quickly due to the low attenuation and high nonlinearity of C_6H_6. The spectrum is shaped after about 2.7 cm of propagation and extended until 12 cm in length of the fiber.

The proposed C_6H_6-core PCFs have the potential for all-fiber robust compact all-fiber SC systems if low-power pump pulses are considered. As observed in Table 1, C_6H_6-PCF in Ref. 11 uses a peak power 122 times larger than those injected into our normal-dispersion fiber, but the spectrum band also only approximates our work and covers the range from 0.7 to 2 μm. For the rest fiber, the soliton-induced SC generation exhibits a relatively limited spectral range compared with 3.35 μm of the broadband SC in Fiber 2. Here, the input power has been reduced to 18.5 kW and is higher than that of this work 23 times. Ultrashort pulse duration and high pulse peak power are the domain of complex optical parametric chirped-pulse amplification (OPCPA) systems that usually operate with kHz repetition rates, resulting in decreased coherence. The coupling efficiency of high-power laser pulses into the small fibers is low. In addition, high peak power may lead to fiber damage via the thermal effects of laser pulses on the input fiber end and lead to high error in SC simulation with the use of the split-steps method. In contrast, the proposed fibers can offer broad SC generation with much lower input peak power (450 and 789 W). Noticeably, the spectrum broadening in Ref. 16 is still limited even with identical peak power values as ours. On the other hand, we prove that the short length of sample fiber can minimize loss and cost during fabrication.

4. Conclusion

We reported on the all-normal and anomalous dispersion SC in the C_6H_6-core fibers. The SC spectrum from 0.72 to 1.82 μm is achieved with 40 fs pulse duration and 18 pJ energy, i.e., input power of 450 W at 1.3 μm central wavelength for Fiber 1. Whereas, Fiber 2 allows to reach SC spectrum in the range of 0.78–4.13 μm in 10 dB dynamics. The spectral band obtained herein is much wider than the SC reported for liquid-core PCFs.[11,16–21] The high nonlinear coefficient associated with the small effective mode area and the relatively low loss contribute significantly to the great SC spectral width of two proposed fibers. This is thanks to our new design, where the diameter of air holes in the first ring near the core is different from the remaining rings.

All proposed fibers are good candidates for compact all-fiber SC systems operating with low-power pump lasers. This would be a cost-effective alternative to glass core fibers since the nonlinearity of C_6H_6 is higher than that of SiO_2. Note that the all-fiber systems are robust, shock-proof and neither comprise axis adjustment mechanics nor additional pulse compressors. The proposed remedy may partially solve

the issues related to the fusion splicing of liquid core PCFs and standard silica fibers. With high coherence all-normal SC, Fiber 1 is found to be suitable for several applications with high pulse-to-pulse coherence such as multi-beam pump-probe technique, pulse compression and temporally synchronized ultra-fast amplifiers with small noise. On the other hand, fibers with anomalous dispersion can be very useful for applications that require a wide spectrum of bandwidth, e.g., gas or liquid sensing, Mach-Zender interferometer and optical coherence tomography.

References

1. M. A. Fakhri *et al.*, *Sci. Rep.* **13**, 5680 (2023).
2. J. C. Knight *et al.*, *Opt. Lett.* **21**, 1547 (1996).
3. Y. Ma *et al.*, *Materials* **15**, 1558 (2022).
4. B. Debord *et al.*, *Fibers* **7**, 16 (2019).
5. P. Saha, S. Majety and M. Radulaski, *Sci. Rep.* **13**, 4112 (2023).
6. L. T. B. Tran *et al.*, *Photon. Lett. Poland* **12**, 106 (2020).
7. S. J. Raja, S. S. Rao and R. Charlcedony, *SN Appl. Sci.* **2**, 499 (2020).
8. Y. Huang *et al.*, *Sensors* **20**, 135 (2020).
9. Y. Wang, R. Gao and X. Xin, *Opt. Express* **29**, 19703 (2021).
10. A. Ghanbari and S. Olyaee, *Crystals* **13**, 226 (2023).
11. C. V. Lanh *et al.*, *Opt. Eng.* **60**, 116109 (2021).
12. C. Stephen *et al.*, *Opt. Express* **26**, 33604 (2018).
13. C. V. Lanh *et al.*, *Opt. Commun.* **537**, 129441 (2023).
14. L. Mohr-Weidenfeller *et al.*, *Nanomanu. Metrol.* **4**, 149 (2021).
15. Y. Zhang, K. Gao and Y. Fan, *Micro Nano Lett.* **14**, 211 (2019).
16. N. T. Thuy *et al.*, *J. Opt.* **51**, 678 (2022).
17. G. Fanjoux *et al.*, *J. Opt. Soc. Am. B* **34**, 1677 (2017).
18. L. V. Hieu *et al.*, *Opt. Quantum Electron.* **53**, 187 (2021).
19. L. V. Hieu *et al.*, *Appl. Opt.* **60**, 7268 (2021).
20. M. Chemnitz *et al.*, *Nat. Commun.* **8**, 42 (2017).
21. M. Chemnitz *et al.*, *Optica* **5**, 695 (2018).
22. H. V. Thuy *et al.*, *Opt. Mater. Express* **11**, 3568 (2018).
23. K. Saitoh *et al.*, *Opt. Express* **11**, 843 (2003).
24. H. T. Duc *et al.*, *Sci. Technol. Dev. J.* **25**, 2581 (2022).
25. Market Study: Benzene, 2nd edn., Ceresana, Accessed on 2 October 2015.
26. T. L. Myers *et al.*, *Appl. Spectrosc.* **72**, 535 (2018).
27. A. A. Voronin and A. M. Zheltikov, *Sci. Rep.* **7**, 46111 (2017).
28. S. Kedenburg *et al.*, *Opt. Mat. Express* **2**, 1588 (2012).
29. C. Strutynski *et al.*, *Adv. Funct. Mater.* **31**, 2011063 (2021).
30. H. V. Le *et al.*, *Opt. Express* **29**, 39586 (2021).
31. https://www.fluigent.com/research/instruments/.
32. S. Kedenburg *et al.*, *Opt. Express* **23**, 8281 (2015).
33. K. Ito *et al.*, *SEI Tech. Rev.* **86**, 51 (2018).
34. H. D. Quang *et al.*, *Appl. Opt.* **57**, 3738 (2018).
35. O. Melchert and A. Demircan, *SoftwareX* **20**, 101232 (2022).
36. A. S. Bezgabadi and M. A. Bolorizadeh, *Opt. Quantum Electron.* **54**, 698 (2022).
37. C. V. Lanh *et al.*, *Opt. Quantum Electron.* **54**, 840 (2022).
38. N. T. Thuy Nguyen Thi, H. T. Duc and C. V. Lanh, *Opt. Quantum Electron.* **55**, 93 (2023).
39. A. Sharafali and K. Nithyanandan, *Appl. Phys. B* **126**, 55 (2020).